Ferroelectric nematic liquid crystal thermomotor

Marcell Tibor Máthé,[1,2] Ágnes Buka,[1] Antal Jákli,[1,3,4] and Péter Salamon [1,*]

[1]*Institute for Solid State Physics and Optics, Wigner Research Centre for Physics, P.O. Box 49, Budapest H-1525, Hungary*
[2]*Eötvös Loránd University, P.O. Box 32, H-1518 Budapest, Hungary*
[3]*Materials Sciences Graduate Program and Advanced Materials and Liquid Crystal Institute, Kent State University, Kent, Ohio 44242, USA*
[4]*Department of Physics, Kent State University, Kent, Ohio 44242, USA*

A thermal gradient-induced circular motion of particles placed on ferroelectric nematic liquid crystal sessile drops is demonstrated and explained. Unlike hurricanes and tornadoes that are the prime examples for thermal motors and where turbulent flows are apparent, here the texture without tracer particles appears completely steady indicating laminar flow. We provide a simple model showing that the tangential arrangement of the ferroelectric polarization combined with the vertical thermal gradient and the pyroelectricity of the fluid drives the rotation of the tracer particles that become electrically charged in the fluid. These observations provide a fascinating example of the unique nature of fluid ferroelectric liquid crystals.

I. INTRODUCTION

In solid ferroelectrics, large pyroelectric coefficients and bound charge accumulations could be observed as a result of gradients of composition [1–4], strain [5], or temperature [6,7]. Dipole vortices were found in nanoscale solid state systems of ferromagnetic and ferroelectric materials that promise new applications as nanomemories, sensors, and transducers [8]. Vortexlike topological structures of dipoles that exhibit toroidal moments [9–12] were predicted and found in nanoparticles [13–16], nanocomposites [17], thin films [18,19] of ferroelectrics, and in a metamaterial [20].

Solid ferroelectrics do not have mobile ionic charges, therefore, it is an interesting question, whether fluid ferroelectrics with mobile ionic contaminations can produce similar phenomena. Three-dimensional fluid ferroelectric nematic (N_F) materials have been observed recently in liquid crystals (LCs). The N_F LC phase is the newest form of nematic (N) LCs that are uniaxial anisotropic fluids which can be reversibly reoriented with electric fields, making nematics the essential elements of the dominant technology for electronic information devices, such as today's flat panel displays. Whereas in normal dielectric nematic liquid crystals the average molecular axis, the director $\hat{n}$, has a head-tail symmetry, i.e., $\hat{n} = -\hat{n}$, in ferroelectric nematic liquid crystals the director is a vector $\vec{n}$, which is parallel to the average molecular dipole density the macroscopic polarization $\vec{P_s}$. Although it was predicted by Born already in 1916 [21,22], there were no unambiguous experimental indications of a fluid ferroelectric nematic phase until the syntheses of the highly polar rod-shaped compounds referred to, respectively, as DIO and 4-[(4-nitrophe-noxy)carbonyl]phenyl2,4-

dimethoxybenzoate (RM734) by Nishikawa *et al.* [23] and Mandle *et al.* [24,25] in 2017. These materials have a large molecular dipole moment of about 10 D, a ferroelectric polarization up to 5 μC/cm^2 and as high as $\varepsilon \sim 10^4$ dielectric permittivity. The N_F phase of RM734 was first suggested to have splayed polar order [26–28], but more recently it was shown that it has a uniform ferroelectric nematic phase [29].

Here we show that both the appearance of the polarization gradient-induced bound charges and the vortex structure observed in solid ferroelectrics can manifest themselves in the form of thermal gradient-induced circular motion of particles placed on ferroelectric nematic liquid crystal drops. In contrast to hurricanes, tornadoes, heat powered turbines and geothermal pumps that are prime examples for thermal motors and where turbulent motions are apparent, here the texture without tracer particles appears completely steady indicating laminar flow. We will show that the tangential arrangement of the ferroelectric polarization combined with the vertical thermal gradient and the pyroelectricity of the fluid drives the rotation of the tracer particles that become electrically charged in the fluid.

II. EXPERIMENTAL RESULTS

In our studies, we used the previously reported compound RM734 [24–27,29]. The flat glass substrates, served as base plates of the sessile droplets, were spin coated by a polyimide (JALS204, JSR, Japan) providing perpendicular orientation of director to the surface in the nematic phase. The sessile droplets were prepared in a custom-made setup with heated environment and micromanipulators. The experiments were carried out by using a Leica DMRX polarizing microscope equipped with a Linkam LTS350 hot stage and a TMS94 controller providing a temperature stability of 0.01 °C.

Polarized optical microscopy images of sessile submillimeter diameter drops of RM734 heated from the bottom are

*Author to whom correspondence should be addressed: salamon.peter@wigner.hu
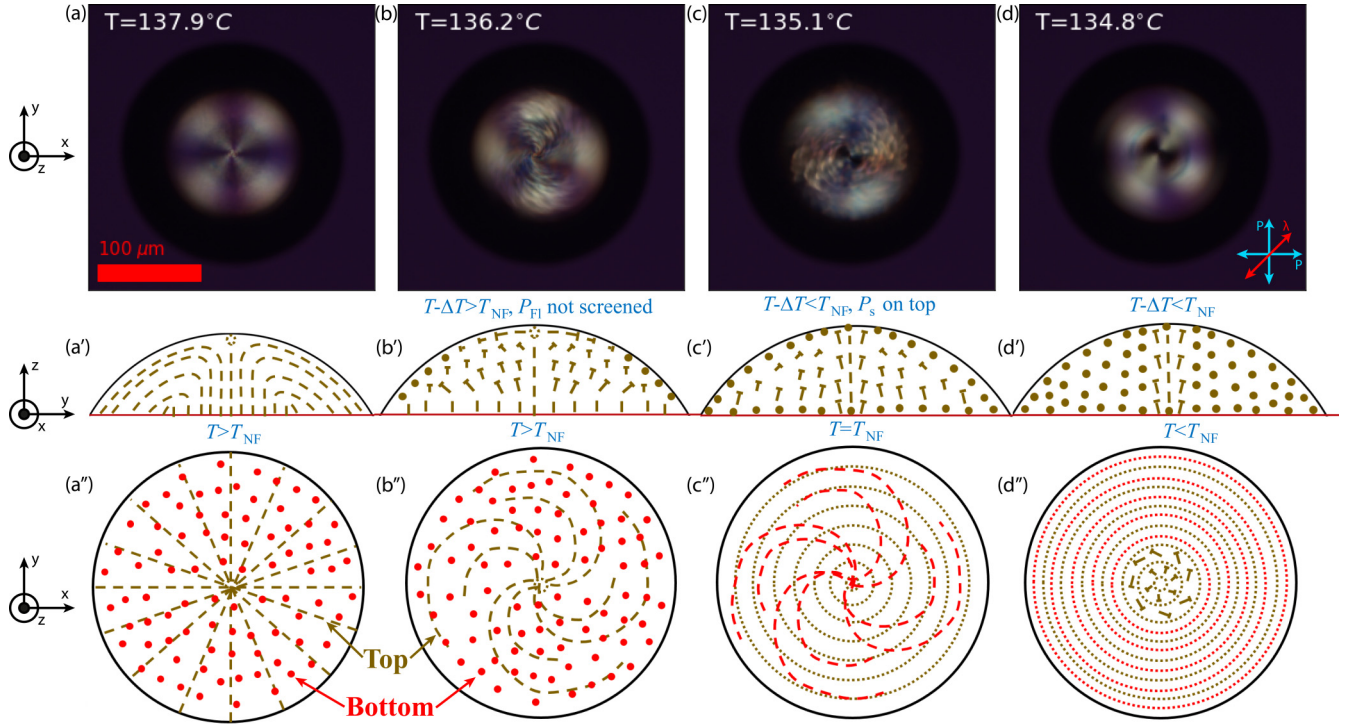
FIG. 1. Polarizing optical micrographs and structures of the sessile drop around the $N \to N_F$ transition. Top temperature: $T - \Delta T$, bottom temperature: T. (a) Radial director structure in the N phase ($T - \Delta T > T_{N_F}$). The top temperature approaches (b), then goes below T_{N_F} (c). The entire drop is in the N_F phase (d). The primed and double primed figures show the corresponding side and top cross sections of the director structure, respectively.

shown in Fig. 1 at four different temperatures near the N-N_F transition.

In the N phase, the director is perpendicular to the solid substrate ("homeotropic" alignment) achieved by a thin polyimide coating and verified by independent measurements in sandwich cells. The four-brush texture seen in Fig. 1(a) corresponds to a radial director structure with a central defect at the top and a parallel (or tilted) director at the upper curved interface as sketched in Figs. 1(a′) and 1(a″). For simplicity, we display the parallel director there. When the colder top approaches T_{N_F}, the splay elastic constant K_{11} decreases, presumably due to the presence of a flexoelectric (Fl) polarization $\vec{P}_{Fl} = e_1 \hat{n} (\vec{\nabla} \cdot \hat{n})$ induced by the splay of the radial director structure [27]. If $\vec{P}_{Fl}$ is large enough, the radial flexoelectric polarization cannot be screened by free charges anymore. Consequently, an internal (in) electric field $\vec{E}_{in} = -\frac{\vec{P}_{Fl}}{\varepsilon_o \varepsilon_\parallel}$ forms that enforces a spiraling director distribution at the top to prevent the polarization from ending in an insulating surface, leading to the texture and director structures seen in Figs. 1(b), 1(b′), and 1(b″). Further cooling through the $N \to N_F$ transition at the colder top, a ferroelectric polarization $\vec{P}_s$ is generated leading to an internal field $\vec{E}_{in} = -\frac{\vec{P}_s}{\varepsilon_o \varepsilon_\parallel}$, and the polarization field becomes tangential. Such a texture and the sketch of the corresponding director configuration are seen in Figs. 1(c), 1(c′), and 1(c″). As the ferroelectric phase reaches the bottom, the polar homeotropic surface orientation would result in an internal field that turns the director and the polarization tangentially in the entire droplet except in the vicinity of the central defect. This texture and the corresponding

director structures are seen in Figs. 1(d), 1(d′), and 1(d″). Note that by using the apparent temperature difference of the phase transitions on the top [Fig. 1(b)] and on the bottom [Fig. 1(c)] combined with the known height of the droplet (47 μm), we can estimate the temperature gradient as 23 mK/μm.

Polarimetric measurements of RM734 in cylindrical basins of about 850 nm depth support the above scenario. A custom modification of our polarizing microscope allowed polarimetric measurement using tunable liquid crystal retarders [30] providing two dimensional spatial maps of the average director field and the magnitude of optical retardation due to birefringence. The distribution of the average director is represented by a field of green rods in Fig. 2. The initial radial configuration [Fig. 2(a)] starts to be spiraling, and at the same time, the increase in retardation [Fig. 2(b)] indicates that the homeotropic region at the bottom shrinks whereas still being in the N phase. In the polar phase, the director becomes tangential in the entire drop [Fig. 2(c)] except near the central defect where the reduced retardation suggests that the director remains homeotropic in the middle.

In one drop, we observed a few micrometer diameter particle, which is at rest in the N phase but starts circulating when it is cooled from the N to the N_F phase. The circular flow starts immediately, as soon as the upper part of the drop went under the phase transition as seen in Supplemental Material Video 1 [31]. Then 8 μm diameter buoyant polystyrene microspheres (Sigma-Aldrich) were intentionally placed on the drops as tracers. Even larger clusters of particles were able to circulate as floating on the droplets (see Supplemental Material Video 2 [31]). The rotation at constant 131 °C in the N_F phase is
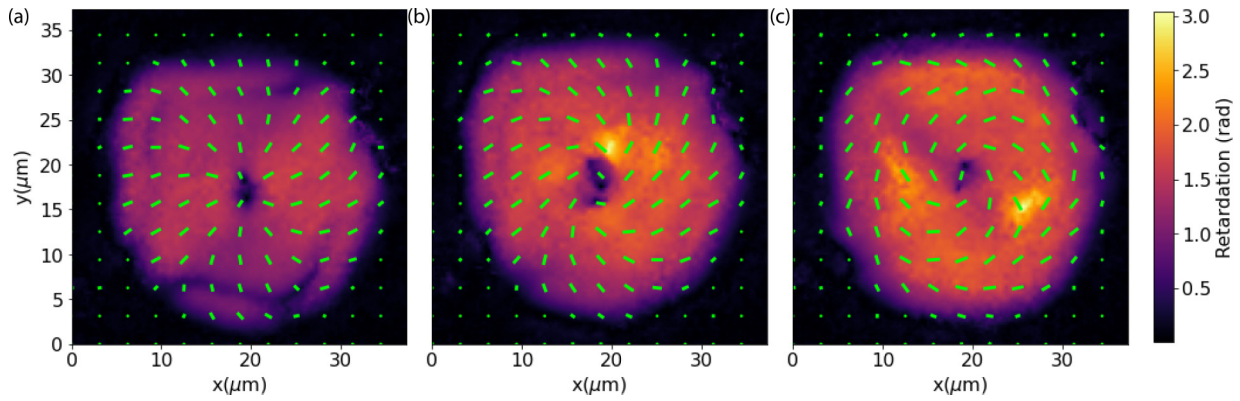
FIG. 2. The retardation of a thin disc of RM734. (a) at 140 °C in the nematic phase, (b) at 134 °C close to the N-N_F transition, (c) at 127 °C in the N_F phase. The green rods represent the averaged orientation of the director.

illustrated in Figs. 3(a)–3(d) by showing snapshots of the drops with the particles on their top. The height of the droplet in this example was 66 μm. The green and yellow arrows pointing to two clusters help to follow the clockwise motion around the central part of the droplet where a topological defect is located.

We noted that the presence of a vertical temperature gradient plays key role in the circular flow found in the ferroelectric droplets. The following experimental observations support this hypothesis: (1) keeping the bottom substrate at a constant temperature whereas cooling the top increases the speed of rotation; (2) turning the drops upside down results in opposite rotation direction; (3) increasing the temperature at the

top by a transparent heater allows to completely stop and even to invert the circulation; then turning off the top heater restores the original state as seen in Supplemental Material Video 3 [31].

The angular velocity of the rotation is found to increase with larger thermal gradient across the drop, whereas the LC director appears to be at rest. This is in contrast to the famous Lehmann rotation of chiral nematic liquid crystal drops where the molecular orientation rotates under a thermal gradient [32,33].

The rotation direction is random from one drop to another (see Supplemental Material Video 2 [31]), but it remains the same if the material does not undergo a phase transition. When
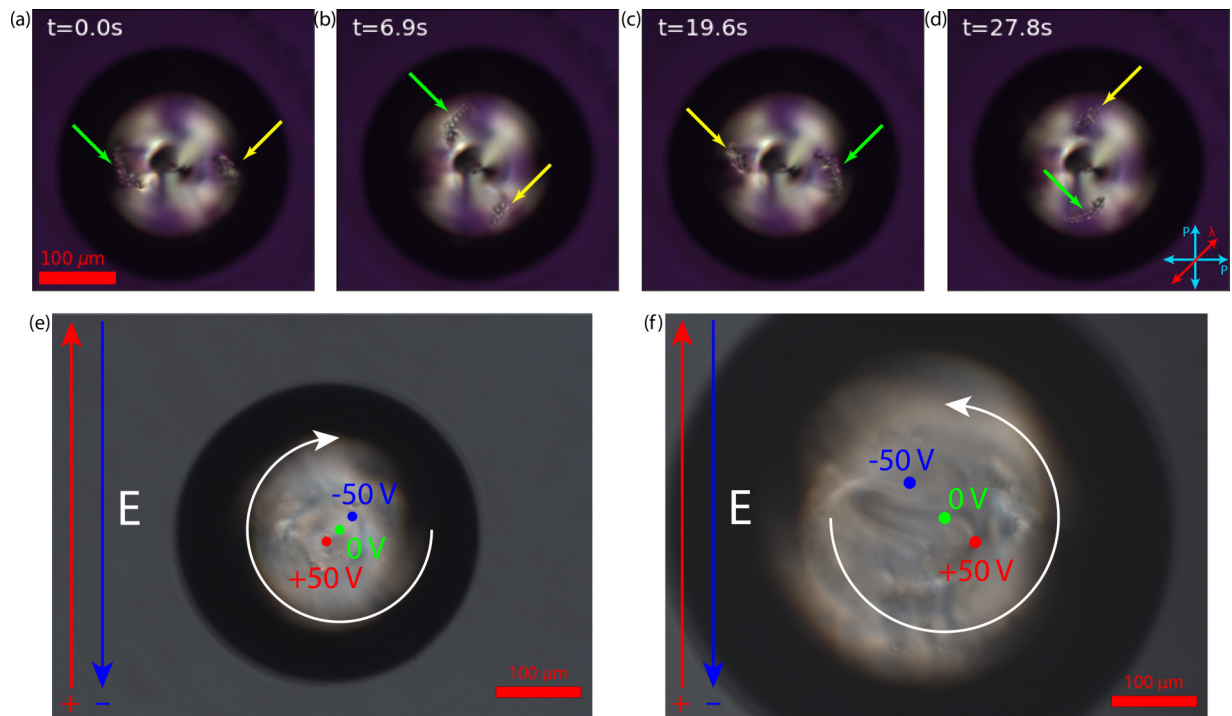
FIG. 3. Time series of snapshots of a sessile droplet of RM734 (at 131 °C in the ferroelectric nematic phase) taken in a polarizing microscope with crossed polarizers and (a)–(d) tint plates. The two arrows indicate two groups of tracer particles following a circular orbit around a central defect. In-plane DC electric field induced displacement of the central defect core (indicated by colorful dots) subjected to ±50 V in the case of two droplets: with (e) clockwise and (f) counterclockwise flow.
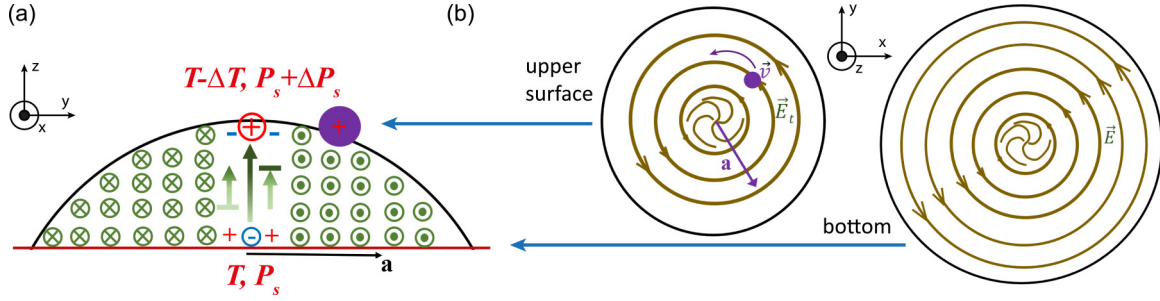
FIG. 4. (a) Side view and (b) top view sketches of a ferroelectric nematic droplet in a vertical temperature gradient leading to a tangential electric field and material flow.

heating up and cooling down again to the ferroelectric phase, the direction of the rotation may change. The speed of rotation is lower for smaller droplets. In some bigger droplets, two defects could be observed, and in those cases, the rotation was observable around the defect cores with opposite direction as seen in Supplemental Material Video 4 [31].

The circulation is found to exist as long as the temperature gradient is maintained, although we experienced a decay of the rotation speed of the particles after several hours, e.g., about 40% in 4 h. This may be attributed to the metastability of vortex states reported in small ferroelectric capacitors of circular confinement [34] due to magnetic induction ($\vec{\nabla} \times \vec{D} = -\frac{d\vec{B}}{dt}$) and the chemical degradation of the material upon long term thermal exposure.

A further important experimental finding indicated that the positions of the upper defect cores can be affected by DC electric fields applied on the sample plane using linear surface electrodes (placed 1 mm away from each other). In the distinct droplets presented in Figs. 3(e) and 3(f), we can see two spectacular features. The first is that the defect cores are displaced on the sample plane in a direction not parallel but at an angle of about 45° with respect to the external electric field. The displacement direction depends on the sign of the field as well as on the direction of the circular flow as seen in Figs. 3(e) and 3(f). Our experiments indicated negative charge accumulation in the top defects in the observed droplets. Finally, when we applied DC electric field in vertical direction across the drop, we could occasionally observe the flipping of rotation direction. Furthermore, in case of large droplets (see a 1.4 mm diameter droplet in Supplemental Material Video 5 [31]), we observed circular motion of defect lines in the ferroelectric phase indicating stationary rotational flow without continuous director rotation, which is not due to the presence of tracer particles.

III. DISCUSSION

Cross effects, including thermomechanical coupling, were predicted theoretically in the polar nematic phase, however, their specific physical mechanism and their experimental significance have not been clarified yet [35]. Here we propose the following model to describe the experimental findings presented above. The key is to consider a sharp increase in the magnitude of the spontaneous polarization $|\vec{P}_s|$ on cooling below the $N \rightarrow N_F$ phase transition [29]. According to our experiments, $\vec{P}_s$ lies along the vertical axis in the middle of

the ferroelectric droplets as being parallel to the homeotropic director in the vicinity of the central defect. Consequently, a vertical temperature gradient (assuming a colder top) results in a higher polarization that leads to an extra (let us assume positive) bound charge (volume) density at the central top, given by $\rho_v = -\vec{\nabla} \cdot \vec{P}_s$ [36]. Radially outwards from the defect, the director becomes tangential, that leads to an annular field of polarization that results in an internal electric field $\vec{E}_{in} = -\frac{\vec{P}_s}{\varepsilon_o \varepsilon_{\parallel}}$ which has a finite rotation $\vec{\nabla} \times \vec{E}_{in} = -(\varepsilon_o \varepsilon_{\parallel})^{-1} \vec{\nabla} \times \vec{P}_s \neq 0$ in the N_F phase (see Fig. 4). Note that in ferroelectric nematic materials as for RM734, the ferroelectric polarization strongly increases on cooling below the N-N_F transition (pyroelectricity), resulting in a rotation that is faster at a larger temperature gradient. Ionic contaminants as mobile charges of the opposite sign need to compensate the central pyroelectric bound charge; therefore, a radial charge separation occurs and the region further from the defect becomes richer in positive charges. The tangential electric field can exert a force on the charges to follow an orbit around the defect. The drag force induced by the charged molecules on neutral fluid elements can result in global flow in the droplet.

Let us consider now a simplified explanation of the tangential movement of tracer particles. Neglecting any acceleration of the particles as a crude approximation, we can write that the electric and viscous drag forces acting on a particle orbiting at a radius a, are in balance: $q_p \vec{E}_t = -\vec{F}_{drag} \approx 6\pi \eta \vec{v} R$, where $q_p, \vec{E}_t, \eta, \vec{v}$, and R are the charge of the particle, the effective electric field, the viscosity, the particle velocity, and radius, respectively. According to Poisson's equation, the depolarizing electric field is $\vec{E}_t = -\frac{\vec{P}_s}{\varepsilon_o \varepsilon_{\parallel}}$ [37]. The charge at the particle is proportional to the bound charge as $q_p \propto -\xi(a) \frac{\partial P_s}{\partial T} \frac{\partial T}{\partial z} V_c$, where $\xi(a)$, $p = \frac{\partial P_s}{\partial T}$, $\frac{\partial T}{\partial z}$, and V_c are a quotient related to the radius dependent charge distribution, the pyroelectric coefficient, the vertical temperature gradient, and the effective contact volume of the particle, respectively. Assuming that V_c is proportional to the product of the contact area and a penetration depth as $V_c = R^2 A_c$, after staightforward calculations, we get an estimate on the angular frequency ω of the particle movement as $\omega \propto \frac{\xi(a)}{a 6\pi \eta} \frac{|\vec{P}_s|}{\varepsilon_o \varepsilon_{\parallel}} p \frac{\partial T}{\partial z} A_c R$. This model is obviously oversimplified, but it captures the main feature of our experimental findings, namely, that the circular flow requires the presence of spontanous polarization, and the rotation speed is proportional to the temperature gradient. Considering the parameters: $R = 4\,\mu m$, $A_c = 1\,\mu m$, $\eta = 1$ Pa s [26],

$\varepsilon_{\parallel} = 10^4$, $a = 80\,\mu$m, $\delta z = 10\ \mu$m, $T = 130\,^\circ$C, $\delta T = 1\,^\circ$C, $|\vec{P}_s| = 2.7\,\mu$C/cm^2 [29], $\delta|\vec{P}_s| = 0.4\ \mu$C/cm^2, and $\xi = 0.5$, we get similar angular velocity ($\omega = 0.16$ s^{-1}) as that found in the experiments.

The oblique displacement of defects in electric fields can be explained by the interaction of the top pyroelectric charge with the local electric field, which is the sum of the external field and the tangential field due to the vortex of spontaneous polarization. This explains the dependence of displacement direction on both the sign of the external field and the helicity of the circular flow as well. Flipping the vertical polarization at the defect using vertical DC electric field would invert the sign of the bound charge according to the model described above. In case of an unchanged tangential polarization, this would lead to the inversion of orbiting direction. In our experiments, however, we found only an occasional reversal of circulation upon applying vertical DC electric fields. We can understand this by considering that the applied field oriented the director (and the polarization) not only at the defect, but in regions of tangential orientation as well. After switching off the external field, the direction of annular polarization is randomly selected, similar to the case when cooling from the nematic to the ferroelectric phase.

[1] J. V. Mantese, N. W. Schubring, A. L. Micheli, and A. B. Catalan, Ferroelectric thin films with polarization gradients normal to the growth surface, Appl. Phys. Lett. **67**, 721 (1995).

[2] J. V. Mantese, N. W. Schubring, A. L. Micheli, A. B. Catalan, M. S. Mohammed, R. Naik, and G. W. Auner, Slater model applied to polarization graded ferroelectrics, Appl. Phys. Lett. **71**, 2047 (1997).

[3] F. Jin, G. W. Auner, R. Naik, N. W. Schubring, J. V. Mantese, A. B. Catalan, and A. L. Micheli, Giant effective pyroelectric coefficients from graded ferroelectric devices, Appl. Phys. Lett. **73**, 2838 (1998).

[4] M. Marvan, P. Chvosta, and J. Fousek, Theory of compositionally graded ferroelectrics and pyroelectricity, Appl. Phys. Lett. **86**, 221922 (2005).

[5] Y. Zheng, B. Wang, and C. H. Woo, Effects of strain gradient on charge offsets and pyroelectric properties of ferroelectric thin films, Appl. Phys. Lett. **89**, 062904 (2006).

[6] Q. Zhang and I. Ponomareva, Microscopic Insight into Temperature-Graded Ferroelectrics, Phys. Rev. Lett. **105**, 147602 (2010).

[7] Q. Zhang and I. Ponomareva, Depolarizing field in temperature-graded ferroelectrics from an atomistic viewpoint, New J. Phys. **15**, 043022 (2013).

[8] Y. Zheng and W. J. Chen, Characteristics and controllability of vortices in ferromagnetics, ferroelectrics, and multiferroics, Rep. Prog. Phys. **80**, 086501 (2017).

[9] N. Talebi, S. Guo, and P. A. Van Aken, Theory and applications of toroidal moments in electrodynamics: Their emergence, characteristics, and technological relevance, Nanophotonics **7**, 93 (2018).

[10] V. M. Dubovik and V. V. Tugushev, Toroid moments in electrodynamics and solid-state physics, Phys. Rep. **187**, 145 (1990).

[11] S. Prosandeev, I. Ponomareva, I. Kornev, I. Naumov, and L. Bellaiche, Controlling Toroidal Moment by Means of an Inhomogeneous Static Field: An *Ab Initio* Study, Phys. Rev. Lett. **96**, 237601 (2006).

[12] S. Prosandeev, I. Ponomareva, I. Kornev, and L. Bellaiche, Control of Vortices by Homogeneous Fields in Asymmetric Ferroelectric and Ferromagnetic Rings, Phys. Rev. Lett. **100**, 047201 (2008).

[13] M. G. Stachiotti and M. Sepliarsky, Toroidal Ferroelectricity in PbTiO$_3$ Nanoparticles, Phys. Rev. Lett. **106**, 137601 (2011).

[14] E. Durgun, P. Ghosez, R. Shaltaf, X. Gonze, and J. Y. Raty, Polarization Vortices in Germanium Telluride Nanoplatelets: A Theoretical Study, Phys. Rev. Lett. **103**, 247601 (2009).

[15] I. I. Naumov, L. Bellaiche, and H. Fu, Unusual phase transitions in ferroelectric nanodisks and nanorods, Nature (London) **432**, 737 (2004).

[16] I. Naumov and H. Fu, Vortex-to-Polarization Phase Transformation Path in Ferroelectric Pb(ZrTi)O$_3$ Nanoparticles, Phys. Rev. Lett. **98**, 077603 (2007).

[17] Y. Nahas, S. Prokhorenko, L. Louis, Z. Gui, I. Kornev, and L. Bellaiche, Discovery of stable skyrmionic state in ferroelectric nanocomposites, Nat. Commun. **6**, 8542 (2015).

[18] N. Balke, B. Winchester, W. Ren, Y. H. Chu, A. N. Morozovska, E. A. Eliseev, M. Huijben, R. K. Vasudevan, P. Maksymovych, J. Britson, S. Jesse, I. Kornev, R. Ramesh, L. Bellaiche, L. Q. Chen, and S. V. Kalinin, Enhanced electric conductivity at ferroelectric vortex cores in BiFeO$_3$, Nat. Phys. **8**, 81 (2012).

[19] S. Chen, S. Yuan, Z. Hou, Y. Tang, J. Zhang, T. Wang, K. Li, W. Zhao, X. Liu, L. Chen, L. W. Martin, and Z. Chen, Recent progress on topological structures in ferroic thin films and heterostructures, Adv. Mater. **33**, 2000857 (2021).

[20] T. Kaelberer, V. A. Fedotov, N. Papasimakis, D. P. Tsai, and N. I. Zheludev, Toroidal dipolar response in a metamaterial, Science **330**, 1510 (2010).

[21] M. Born, Uber anisotrope Flussigkeiten: Versuch einer Theorie der flussigen Kristalle und des elektrischen Kerr-Effekts in Flussigkeiten, Sitzungsber. Preuss. Akad Wiss **30**, 614 (1916).

[22] O. D. Lavrentovich, Ferroelectric nematic liquid crystal, a century in waiting, Proc. Natl. Acad. Sci. USA **117**, 14629 (2020).

[23] H. Nishikawa, K. Shiroshita, H. Higuchi, Y. Okumura, Y. Haseba, S. I. Yamamoto, K. Sago, and H. Kikuchi, A fluid liquid-crystal material with highly polar order, Adv. Mater. **29**, 1702354 (2017).

[24] R. J. Mandle, S. J. Cowling, and J. W. Goodby, A nematic to nematic transformation exhibited by a rod-like liquid crystal, Phys. Chem. Chem. Phys. **19**, 11429 (2017).

[25] R. J. Mandle, S. J. Cowling, and J. W. Goodby, Rational design of rod-like liquid crystals exhibiting two nematic phases, Chem. Eur. J. **23**, 14554 (2017).

[26] A. Mertelj, L. Cmok, N. Sebastián, R. J. Mandle, R. R. Parker, A. C. Whitwood, J. W. Goodby, and M. Čopič, Splay Nematic Phase, Phys. Rev. X **8**, 041025 (2018).

[27] N. Sebastián, L. Cmok, R. J. Mandle, M. R. De La Fuente, I. Drevenšek Olenik, M. Čopič, and A. Mertelj, Ferroelectric-Ferroelastic Phase Transition in a Nematic Liquid Crystal, Phys. Rev. Lett. **124**, 037801 (2020).

[28] H. Pleiner and H. R. Brand, Spontaneous splay phases in polar nematic liquid crystals, Europhys. Lett. **9**, 243 (1989).

[29] X. Chen, E. Korblova, D. Dong, X. Wei, R. Shao, L. Radzihovsky, M. A. Glaser, J. E. MacLennan, D. Bedrov, D. M. Walba, and N. A. Clark, First-principles experimental demonstration of ferroelectricity in a thermotropic nematic liquid crystal: Polar domains and striking electro-optics, Proc. Natl. Acad. Sci. USA **117**, 14021 (2020).

[30] M. Shribak and R. Oldenbourg, Techniques for fast and sensitive measurements of two-dimensional birefringence distributions, Appl. Opt. **42**, 3009 (2003).

[31] See Supplemental Material at http://link.aps.org/supplemental/10.1103/PhysRevE.105.L052701 for presenting the phase transition from the nematic to the ferroelectric nematic phase in cooling, (SVID1_1Kpermin_cool_1particle.Avi), for pre-senting motion of tracer particles during the phase transition from the nematic to the ferroelectric nematic phase in cooling, (SVID2_cool_clusters.Avi), for presenting motion of tracer particles during the phase transition from the nematic to the ferroelectric nematic phase in cooling, (SVID2_cool_clusters.Avi), for presenting vortex flow around defects, (SVID4_2defects.Avi), and for presenting circular motion of defect lines, (SVID5_defectrot.Avi).

[32] O. Lehmann, Structur, system und magnetisches verhalten flüssiger krystalle und deren mischbarkeit mit festen, Ann. Phys. **307**, 649 (1900).

[33] P. Oswald and A. Dequidt, Measurement of the Continuous Lehmann Rotation of Cholesteric Droplets Subjected to a Temperature Gradient, Phys. Rev. Lett. **100**, 217802 (2008).

[34] A. Gruverman, D. Wu, H. J. Fan, I. Vrejoiu, M. Alexe, R. J. Harrison, and J. F. Scott, Vortex ferroelectric domains, J. Phys.: Condens. Matter **20**, 342201 (2008).

[35] H. R. Brand, H. Pleiner, and F. Ziebert, Macroscopic dynamics of polar nematic liquid crystals, Phys. Rev. E **74**, 021713 (2006).

[36] B. A. Strukov and A. P. Levanyuk, *Ferroelectric Phenomena in Crystals* (Springer, Berlin, Heidelberg, 1998).

[37] A. P. Levanyuk and R. Blinc, Ferroelectric Phase Transitions in Small Particles and Local Regions, Phys. Rev. Lett. **111**, 097601 (2013).